

# Ground states of long-range interacting fermions in one spatial dimension

Zhi-Hua Li

*School of Science, Xi'an Technological University, Xi'an 710021, China*

We explore systematically the ground state properties of one dimensional fermions with long-range interactions decaying in a power law  $\sim 1/r^\alpha$  through the density matrix renormalization group algorithm. By comparing values of Luttinger liquid parameters precisely measured in two different ways, we show convincing evidence that Luttinger liquid theory is valid if  $\alpha$  is larger than some threshold, otherwise the theory breakdown. Combining analysis on structure factor, charge gap and charge stiffness, we determine how the metal-insulator transition point develops as the interaction range is continuously tuned. A region in the range of  $0 \leq \alpha \leq 1$  and small interactions has finite charge gaps, but, interestingly, it shows metallic nature at the same time. From these, we obtain approximate phase diagrams for the entire parameter space and for band fillings equal  $1/2$  and  $1/3$ . Finally, we compare certain bosonization and field theory formula with our quasi-exact numerical results, from which disagreements are found.

## I. INTRODUCTION

One-dimensional (1D) electron models are widely studied due to the viability of various analytical and numerical methods. Typical examples are the Hubbard model and its extensions with short-range (SR) interactions. A dominant theoretical framework for solving and understanding such models is the Luttinger liquid theory<sup>1-3</sup>. In that theory correlation functions decay as non-universal power-laws, with the exponents determined by a single parameter  $K$  (per degree of freedom). However, experiments on quasi-1D systems such as quantum wires<sup>4,5</sup> and carbon nanotubes<sup>6</sup> highlight the importance of long-range (LR) interactions, as in 1D screening is absent and the electrons should interact via the bare Coulomb force. Then the Luttinger liquid theory is not guaranteed to be effective, since it assumes SR interactions.

Schulz<sup>7</sup> applied bosonization method to 1D electron systems with Coulomb force. He found  $4k_F$  density correlation decaying slower than any power laws, thus beyond Luttinger liquid, and interpreted the ground state as a quasi-Wigner crystal. The occurrence of  $4k_F$  (or  $2k_F$  for spinless fermions) wave vector was later examined numerically in continuum<sup>8-11</sup> and discrete models<sup>12,13</sup>.

The systems studied in 7-11 are electrons moving in a continuum (e.g. for electron gas confined in semiconductor heterostructures); when moving on a lattice, they can be localized and form an charge-density-wave (CDW) insulator. The impact of LR interaction on the metal-insulator transition was studied in 14 and 15 using exact diagonalization, and it was shown that the umklapp scattering is reduced in the presence of LR interaction. Regarding the metal-insulator transition, there is a subtle difference between LR spinless and spinfull models that the later seems has no transition for even large interactions<sup>12</sup>.

Despite large amount of work cited in the above, our understandings of 1D LR interacting electrons are still not complete. The widely quoted bosonization formula of near crystalline  $4k_F$  correlation<sup>7</sup> has been rarely unambiguously verified numerically (an exception was in

12); The discussion of the interplay between LR interaction and umklapp scattering was only made for short chains<sup>14</sup>, that need to be checked in large systems; In addition, recent advances in cold atom experiments, such as polar molecular and trapped ions<sup>16</sup>, have realized quasi-1D LR systems with power law interactions  $1/r^\alpha$  and exponent  $\alpha$  broader than a single Coulomb force ( $\alpha = 1$ ), which also worth investigating. Thus improved numerical results are still needed.

In this paper, we study long-range interacting fermions using the density matrix renormalization group (DMRG) algorithms. The model considered here consists of a chain with  $N$  sites,

$$\hat{H} = \sum_i -t(\hat{c}_i^\dagger \hat{c}_{i+1} + h.c.) + \sum_{i < j} \mathcal{V}(|i-j|)(\hat{n}_i - n)(\hat{n}_j - n) \quad (1)$$

where  $\hat{c}_i^\dagger$  ( $\hat{c}_i$ ) is creation (annihilation) operator of a spinless fermion,  $\hat{n}_i$  is a fermion density operator at site  $i$ , and  $n$  is the average density. The interaction potential decays in a power law  $\mathcal{V}(r) = V/r^\alpha$ . The overall amplitude  $V$  is non-negative representing repulsion force. And the exponent  $\alpha$  ranges from  $\infty$  to 0, interpolating continuously nearest neighbour interaction to the unphysical limit of undecayed interaction.

We aim to give a systematic account of the interaction range effects and determine a phase diagram for the full parameter space. The SR limit ( $\alpha = \infty$ ) of Eq.(1) is already well understood. We are particularly interested in whether the Luttinger liquid theory effects for power law interaction when  $\alpha < \infty$ . According to bosonization analysis this should be true if  $\sum_r \mathcal{V}(r)$  is finite<sup>3</sup>, direct numerical evidence is still beneficial, though. We show that when  $\alpha$  is large enough, there is indeed a Luttinger liquid region and its boundary with insulator phase can be determined by the limiting value of the Luttinger parameter. Whereas when  $\alpha$  is small, the system clearly deviates from Luttinger liquid, and the metal-insulator transition can no longer be determined by the Luttinger parameter. In the metallic region the ground state has very slowly decayed density correlation, which is qualitatively consistent with bosonization predictions. However,

the numeric data does not fully match with the analytical ones. We also deliver systematic analysis of the ground state entanglement, which supports conclusions drawn from other quantities.

This work is organized as follows. Sec.II introduces the model and the numerical method; Secs.III and IV determine the phase diagram for band fillings  $n = 1/2$  and  $n = 1/3$ , respectively; Sec.V compares bosonization with our numerical results. Conclusions are drawn in Sec.VI.

## II. METHODS

Except for the hopping amplitude  $t$  (fixed to unity) and filling factor  $n$ ,  $V$  and  $\alpha$  are two main free parameters that we will investigate. Several limiting cases can be noted in the  $V$ - $\alpha$  plane: The line of  $V = 0$  are free fermions. This is also the case for  $\alpha = 0$ . When  $\alpha = \infty$ , Eq.(1) degenerates to the  $t$ - $V$  model (equivalent to the  $XXZ$  model), which is exactly solvable: For half filling there is a metal-insulator transition at  $V_c = 2.0$ . Besides, the low energy field theory for the  $t$ - $V$  model (and other similar models with longer, but finite range, interactions) is the Luttinger model plus a cosine term representing the umklapp scattering, known as the sine-Gordon model. The fixed points for this field theory model are controlled by the Luttinger parameter  $K$ . It is metallic (insulating) if  $K$  is smaller (larger) than a critical value  $K_c$ .  $K_c$  is determined by band filling, which, for spinless fermions, equals  $\frac{1}{2}$  and  $\frac{2}{9}$  at fillings  $n = \frac{1}{2}$  and  $n = \frac{1}{3}$ , respectively.

For generic  $V$  and  $\alpha$ , accurate ground state properties can only be obtained numerically. We use the DMRG algorithm<sup>17</sup> to achieve this. Traditionally, it was difficult to use DMRG to simulate systems with LR interactions. This problem has been solved for the type of LR interaction decaying in a power law in translation invariant systems, due to a technique invented in Ref.18. The basic idea behind of it is to approximating power function with the sum of several exponentials, and encode the Hamiltonian compactly in MPOs (see 18 and 19 for details). Both DMRG and this technique are quasi-exact. In our simulation, the Hamiltonian (1) is represented with the just mentioned technique, using 6 exponentials, and the ground state wave function  $|\psi\rangle$  is represented with matrix product states<sup>20</sup>. Other algorithm details are regular: If not otherwise specified, open boundary conditions (OBC) is used for system size  $N$  ranging from 20 to 1600. Physical quantities are calculated by extrapolation in  $N$ . The quality of the wave function is gauged such that the truncation error to be under  $10^{-9}$  or the variance  $v = \langle \psi | \hat{H}^2 | \psi \rangle - (\langle \psi | \hat{H} | \psi \rangle)^2$  smaller than  $10^{-5}$ . This requires a bond dimension  $D$  of the MPS up to 500.

As we will need to calculate  $K$  in different ways, a variant of DMRG—the iDMRG algorithm<sup>21</sup> is also used in this paper. This algorithm exploits translation invariance and represent the ground state in an infinite matrix product state (iMPS). Since it works directly in ther-

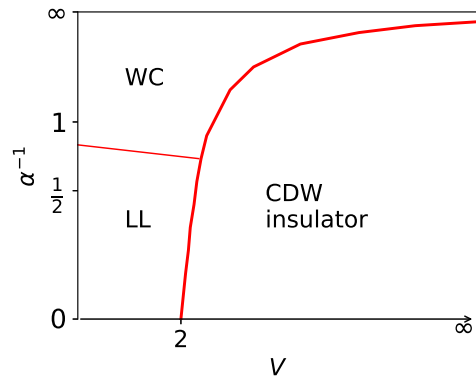


FIG. 1. Schematic phase diagram as a function of the interaction amplitude  $V$  and inverse of exponent  $\alpha$  at  $n = \frac{1}{2}$ . The thick solid line indicates transitions from metallic phases to a CDW insulator phase. This line starts from  $(V, \alpha) = (2.0, \infty)$  and eventually approaches  $\alpha = 0$  when  $V \rightarrow \infty$ . The thin solid line in the metallic regime marks the transition from Luttinger liquid phase (LL) to a Wigner crystal phase (WC). In addition, the ground states for  $V = 0$  or  $\alpha = 0$  corresponds to free fermions and belong to the Luttinger liquid phase.

modynamic limit, no extrapolation in  $N$  is needed and boundary effect is reduced to minimum. Simulations are made and compared with different bond dimensions to ensure accuracy, and the values of the correlators are averaged over one unit cell to enforce better translation invariance.

We study two band fillings  $n = 1/2$  and  $1/3$  which correspond to Fermi wave vectors  $k_F = \pi/2$  and  $\pi/3$ , respectively. For each of them we consider entire range of  $V$  and  $\alpha$ , however, as we will see,  $0 \leq \alpha \leq 3.0$  and moderate  $V$  are revealing enough in practice, so the actual computations is restricted to this range. Our strategy is to analyze starting from the familiar short-range limit ( $\alpha = \infty$ ) and see how phases and quantum critical point (QCP) evolve to unknown regimes when  $\alpha$  is tuned smaller. Because the results for  $n = 1/2$  and  $n = 1/3$  have certain qualitative differences, they are shown separately in below.

## III. $n = 1/2$ PHASE DIAGRAM

Fig.1 shows a schematic phase diagram for  $n = 1/2$ . There are three phases: Luttinger liquid, Wigner crystal and CDW phase. The former two are metallic while the later is an insulator. The Luttinger liquid regime is determined by measuring the Luttinger parameter, as will be explained in subsection III A, where the boundary of it with the CDW phase is located accurately, while the boundary with the Wigner crystal is estimated crudely. The metal-insulator transition point is also determined qualitatively in the whole range of  $\alpha$  by studying the structure factor, charge gap and charge stiffness, as will be presented in III B. These resulting phase boundaries

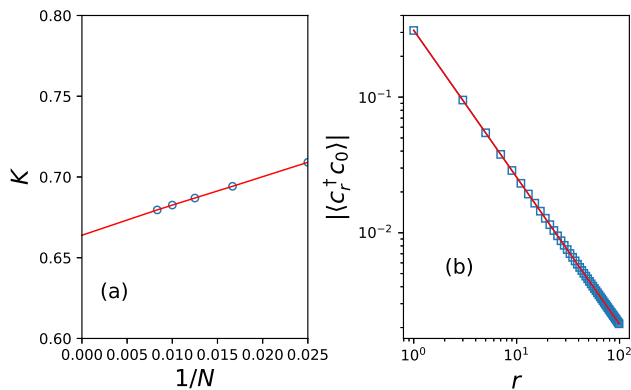


FIG. 2. Correlation exponent  $K$  for  $V = 1.5$  and  $\alpha = 2.5$  extracted through two different methods: (a) By method 1 (see main text): symbols are  $K$  evaluated by Eq.(5) within DMRG versus inverse of system size  $N$ , for  $N = 40, 60, 80, 100$  and  $120$ . The line is a fitting to third order polynomial in  $1/N$ . The extrapolated  $K$  to thermodynamic limit equals  $0.6639$ . (b) By method 2: symbols are single particle Green's function computed using iDMRG with bound dimension  $D = 240$ . The line is fitting of the data to Eq.(3) for  $32 \leq r \leq 60$ . Best fitting is found at  $K = 0.6649$ .

are consistent with the entanglement properties as will be shown in subsection III C.

### A. Luttinger parameter

As mentioned in the introduction, Luttinger liquids are characterized by various power law decaying correlations. For example, the connected density-density correlation and the single particle Green's function are given by the two following formula:

$$\langle (\hat{n}_r - \langle \hat{n}_r \rangle) (\hat{n}_0 - \langle \hat{n}_0 \rangle) \rangle = -\frac{K}{2\pi^2 r^2} + C \frac{\cos(2k_F r)}{r^{2K}} + \dots \quad (2)$$

$$\langle c_r^\dagger c_0 \rangle \sim r^{-\frac{1}{2}(K+K^{-1})} \quad (3)$$

Moreover, the parameter  $K$  in the above two lines are the same one. This prominent character can be used to detect it. Specifically, one may extract  $K$  numerically from Eqs.(2) and (3), then it should be in the Luttinger liquid phase if the two  $K$ s coincide very well, otherwise it falls outside of this phase. We are meant to use that strategy to demarcate the Luttinger liquid phase in the parameter plane. This is feasible provided the numerically extracted  $K$  values are enough accurate. Indeed, due to the high accuracy and versatility of the DMRG like algorithms, Luttinger parameter can be extracted accurately from multiple methods. Two of them which we employ are introduced as follows:

*method 1.* Use DMRG to simulate the ground state and extract  $K$  from Eq.(2)<sup>22</sup>. A direct fitting of the DMRG data with Eq.(2) will face strong end effects. The usual

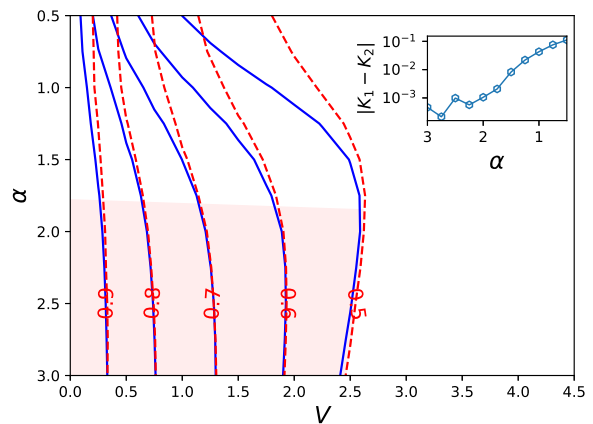


FIG. 3. Contour plot of the correlation exponents  $K_1$  (solid) and  $K_2$  (dashed) on the  $V$ - $\alpha$  plane, with their values restricted to no smaller than  $K_c = 0.5$ . Each value of  $K_1$  ( $K_2$ ) is calculated using the same way as in Fig.2 (a) [(b)]. The shaded region where  $K_1$  and  $K_2$  are nearly identical marks the Luttinger liquid phase. Inset shows the difference of  $K_1$  and  $K_2$  vs.  $\alpha$  on a transect line of  $V = 1.0$ . In this section all results are for  $n = 1/2$ . In the entire paper Figs.2, 3 and 10 used both DMRG and iMPS, Fig.4 used iMPS and all rests used DMRG solely.

conduct is to calculate its Fourier transform, i.e. the static structure factor

$$S(k) = \frac{1}{N} \sum_{i,j} e^{ik(i-j)} (\langle \hat{n}_i \hat{n}_j \rangle - \langle \hat{n}_i \rangle \langle \hat{n}_j \rangle), \quad (4)$$

then  $K$  is given by the slope of  $S(k)$  at zero momentum,

$$K = 2\pi \left. \frac{dS(k)}{dk} \right|_{k=0}. \quad (5)$$

Numerically, this equation can be approximated by  $K = 2\pi[S(2k_1) - S(k_1)]/k_1$ , where  $k_1 = 2\pi/N$  is the smallest momentum for size  $N$ . An example of the extrapolated  $K$  value for thermodynamic limit in this method at  $V = 1.5$  and  $\alpha = 2.5$  is shown in Fig.2(a).

*method 2.* Use iDMRG to calculate the ground state and extract  $K$  from Eq.(3)<sup>23</sup>. Since in the iMPS representation the boundary effect is very small, direct fitting of  $\langle c_r^\dagger c_0 \rangle$  with Eq.(3) suffices to get accurate  $K$ . For small  $r$ , irrelevant operators may affect the scaling, while for large  $r$ , accuracy loses, so an intermediate fitting region of  $32 \leq r \leq 60$  has been used<sup>24</sup>. An example of  $K$  extracted in this method is shown in Fig.2(b).

For clarity, we denote the  $K$ s obtained in the two methods by  $K_1$  and  $K_2$  in order. Contour lines for them in the  $V$ - $\alpha$  plane are drawn together in Fig.3. Good coincidence is found for an extended region in the lower left part of the plane. Regarding that  $K_1$  and  $K_2$  are obtained from different algorithms and different quantities, such a coincidence is very remarkable. This means that for large enough  $\alpha$  the LR interactions are irrelevant at

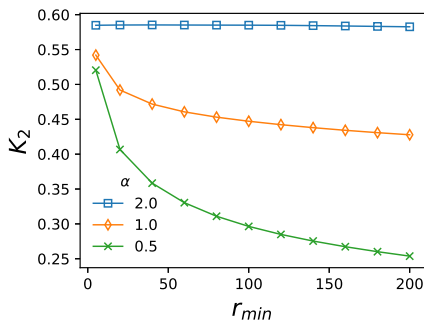


FIG. 4. Correlation exponent  $K_2$  vs.  $r_{min}$  at  $V = 2.0$  and for several values of  $\alpha$ , where  $K_2$  is extracted by fitting iMPS data of the single particle Green's function with Eq.3 for  $r$  in the range  $[r_{min}, r_{min} + 30]$  with varying  $r_{min}$ .

the Luttinger liquid fixed point and that their only effect was a quantitative renormalization of the Luttinger liquid parameters. Either  $K_1$  or  $K_2$  can be taken as the value of Luttinger parameter, since they are very close. Their difference  $\epsilon \equiv |K_1 - K_2|$  can be even taken as an estimate of error, which is about  $10^{-3}$  for  $\alpha \gtrsim 2.0$  (see inset of Fig.3). Nevertheless, since there is no criterion as to how large an  $\epsilon$  would indicate deviation from Luttinger liquid, it is not able to give an accurate  $\alpha_c$  for the upper boundary of this region. By direct observation,  $\alpha_c$  should be between 2.0 and 1.0 and depend slightly on  $V$ . A comparison of this result with bosonization arguments will be given in section V.

Taking account of the backward scattering, the above result also implies that the sine-Gordon model should be still valid for finite  $\alpha$  when  $\alpha > \alpha_c$ . Then the lower half of the limiting contour line  $K_1 = 0.5$  (or  $K_2 = 0.5$ , since they are close and their small discrepancy is caused by logarithm corrections which are not incorporated in Eqs.(2) and (11)) determines unambiguously how the metal-insulator transition point  $V_c$  evolve as  $\alpha$  reduces from 3.0 to  $\alpha_c$ . For reference,  $V_c$  are  $2.45 \pm 0.05$  and  $2.65 \pm 0.05$  for  $\alpha = 3.0$  and 2.0, respectively. Note that they are not far from the critical value of 2.0 for  $\alpha = \infty$ .

In the small  $\alpha$  regime ( $0 < \alpha < \alpha_c$ ) large difference between the two  $K$ s indicates the system is in a new fixed point. In this sense, this is the true LR regime. Both  $K_1$  and  $K_2$  quickly reduces as  $\alpha$  becomes smaller, indicating reinforcement of the density correlation. Here we emphasize that  $K_1$  and  $K_2$  are not well defined ‘‘Luttinger parameter’’ in this regime. They can still be extracted by curve fitting only because marginal Luttinger liquid character is retained. In fact their values are scale dependent. A demonstration of this for  $K_2$  is shown in Fig.4. One can see that, at  $\alpha = 2.0$  (in the Luttinger liquid phase),  $K_2$  is stable against different fitting ranges, meaning Eq.3 is very well satisfied, while at  $\alpha = 1.0$  or 0.5, reduction of  $K_2$  with increasing length scales indicates deviation from Eq.3. This is another evidence for breakdown of Luttinger liquid. Then, considering the backward scattering, the sine-Gordon model should be

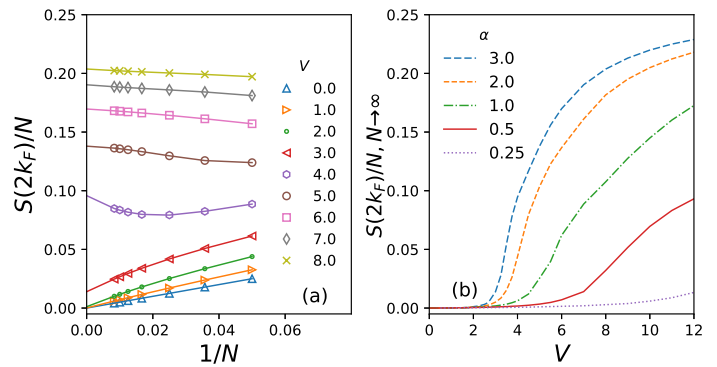


FIG. 5. (a) Scaled static structure factor at  $k = 2k_F$  versus inverse system size for  $\alpha = 3.0$  and different  $V$ . Lines are fit of the data to third order polynomial in  $1/N$ . (b) Extrapolation of  $S(2k_F)/N$  to infinite  $N$  as a function of  $V$  for different  $\alpha$ .

no longer justified either. So there is no reason to expect boundary between metallic and insulating phases given by  $K_c = 0.5$  in this regime.

## B. the metal-insulator transition

For large enough  $V$  (and  $\alpha \neq 0$ ) the potential energy dominates, then the fermions are always expected to form an insulating phase. As stated in the above, the metal-insulator transition point  $V_c$  can be determined by Luttinger parameter only in the large  $\alpha$  regime. In order to see the dependence of the phase boundary on  $\alpha$  in its full range, in below we consider some other quantities.

The metallic phases are translation invariant, while the insulator phase has a CDW order with a wave length equal to inverse of the density of fermion (corresponding to wave number  $k = 2k_F$ ). This  $2k_F$  order can be detected by a non-vanishing  $S(2k_F)/N$  value in thermodynamic limit. The scaling of the structure factor against  $1/N$  for  $\alpha = 3.0$  and several  $V$  is shown in Fig.5(a). For  $V \leq 3.0$ , this quantity is extrapolated to zero or very small values, while clearly becomes finite for larger  $V$ . This behaviour is largely in agreement with  $V_c = 2.45$  obtained by the above study of Luttinger parameter. The extrapolated thermodynamic limit value as a function of  $V$  for different  $\alpha$  is shown in Fig.5(b). For each  $\alpha$ , it changes from zero to finite values at some QCP  $V_c$ , which is not easy to be accurately located. Nevertheless, it is clear that qualitatively the tendency to form CDW order is always weakened as  $\alpha$  reduces.

The next quantity considered is the single particle charge gap<sup>25</sup>. In thermodynamic limit it will normally be zero in metallic phases, while become finite in insulating phases. Its definition is

$$\Delta(N) = E(N_f + 1) + E(N_f - 1) - 2E(N_f), \quad (6)$$

where  $N_f = nN$  is the number of fermions. Scaling of  $\Delta$  with inverse system size at  $\alpha = 3.0$  and 0.5 are shown



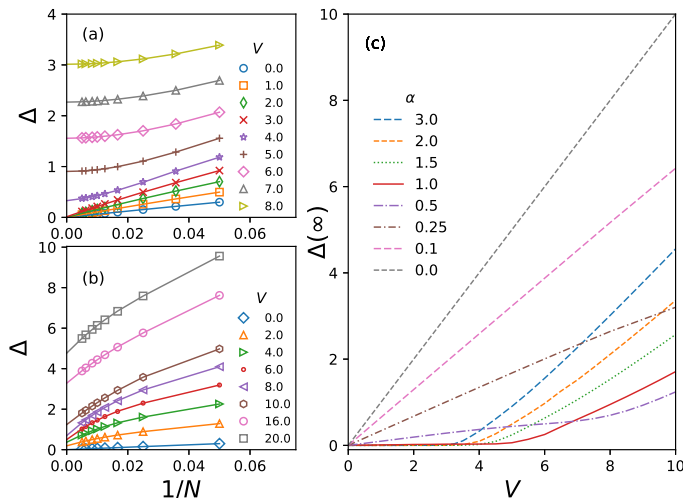


FIG. 6. Single particle charge gap  $\Delta$  versus inverse system size at  $\alpha = 3.0$  (a) and  $\alpha = 0.5$  (b) and for each of them several values of  $V$ . Lines are fit of the data to the function  $\Delta(N) = \Delta(\infty) + a_1 \frac{1}{N} + a_2 \frac{1}{N^2} + a_3 \frac{1}{N^3}$  (c)  $\Delta(\infty)$  extracted from data fitting as a function of  $V$  for different  $\alpha$ .

in Fig.6(a) and (b), respectively, for different interaction strength. Each group of data can be well fitted with third order polynomials in  $1/N$ , leading to certain thermodynamic limit values  $\Delta(\infty)$ . Then the extrapolated  $\Delta(\infty)$  as a function of  $V$  are shown for different  $\alpha$  in Fig.6(c), from which, two distinct behaviours can be observed separated by  $\alpha = 1$ . For each  $\alpha > 1$ ,  $\Delta(\infty)$  changes from zero to finite values at certain critical  $V_c$ , and  $V_c$  should get larger as  $\alpha$  reduces; For each  $0 \leq \alpha \leq 1$ ,  $\Delta(\infty)$  is (almost) proportional to  $V$  in the beginning, and later may still grow linearly in  $V$  but with a larger slope (At  $\alpha = 1$  this is marginal and not very obvious, and, at  $\alpha = 0$ ,  $\Delta(\infty) = V$  holds exactly for all range of  $V$ ).

The gap for  $\alpha > 1$  agrees with previous findings about the Luttinger parameter and scaled structure factor, while the results for  $0 \leq \alpha \leq 1$  and small  $V$  do not: There is no  $2k_F$  CDW order, yet there is a finite charge gap. This raises a question that whether the phase in this regime is a metal or insulator? If we follow the notion of Kohn that metal/insulator should be classified by the ground state wave function alone (while not the spectrum)<sup>26,27</sup>, then it should be metallic, and existence of the charge gap should be understood as one peculiar feature of true LR interaction potential.

Two facts supporting metallic nature of the  $0 \leq \alpha \leq 1$  and small  $V$  regime follow. First, consider the exact solvable region of  $\alpha = 0$ . For them the ground state wave functions are identical to that of the free fermions of  $V = 0$ , and the single particle charge gap can be easily worked out to be  $\Delta(N) = V + 4\pi/N + O(1/N^2)$  for a lattice size  $N$ , which equals  $V$  in thermodynamic limit. This extreme case provides an exact example of a metal with a finite charge gap. Second, for generic  $\alpha$ , we measure

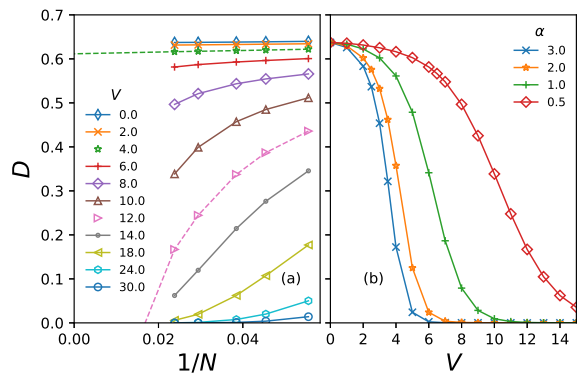


FIG. 7. (a) Charge stiffness  $D$  vs.  $1/N$  at  $\alpha = 0.5$  and for different  $V$ . The system sizes are  $N = 18, 22, 26, 34$  and  $42$ , corresponding to odd numbers of fermions. Solid lines at are guide to eye. Dashed lines at  $V = 4.0$  and  $12.0$  are fit to third order polynomials in  $1/N$ . The former fit is good, while the later leads to negative  $D$  which is clearly incorrect. (b)  $D$  as a function of  $V$  for different  $\alpha$ , obtained at a fixed finite system size of  $N = 42$ . These data are obtained through DMRG with periodic boundary conditions and the bond dimensions used are up to 640.

Kohn's charge stiffness<sup>26</sup>

$$D = N \left. \frac{\partial^2 E(\phi)}{\partial \phi^2} \right|_{\phi_m}, \quad (7)$$

where  $\phi$  is a magnetic flux penetrating periodic ring of model Eq.(1).  $\phi_m$  is the location of minimum of the ground state energy, which equals  $0$  ( $\pi$ ) for an odd (even) number of fermions. Fig.7(a) shows  $D$  vs.  $1/N$  for fixed  $\alpha = 0.5$  and different  $V$ , deep in the LR regime, with  $N$  no larger than  $42^{28}$ . When  $V$  is small or large, finite size effects are weak and extrapolation to infinite  $N$  should be good. For example, at  $V = 4.0$ ,  $D$  is extrapolated to a finite value, showing a metallic state. Similar conclusions can be reached for other  $(V, \alpha)$  pairs when they are both small. For intermediate  $V$ , finite size effects are strong, and extrapolation using small system sizes will lead to large error [see the line at  $V = 12.0$  of Fig.7(a)]. Then we compare  $D$  as a function of  $V$  for different  $\alpha$ , with a fixed finite system size of  $N = 42$ , as shown in Fig.7(b). The function values are always promoted as  $\alpha$  reduces, indicating, for the finite system size, stronger metallic character for smaller  $\alpha$ . This result is consistent with the behaviour of the extrapolated structure factor shown in Fig.5(b).

From the above analysis, we conclude that there are metal-insulator transitions for all  $\alpha > 0$  and the transition point  $V_c$  shifts to larger values as  $\alpha$  reduces ( $V_c$  should go to infinity as  $\alpha$  approaches zero). It means that the fermions are less likely to be localized by the backscattering by the lattice with increasing interaction range. This remarkable fact was uncovered in earlier works of Refs. 14 and 15 for short chains. We confirm this for even larger system sizes and in wider parameter

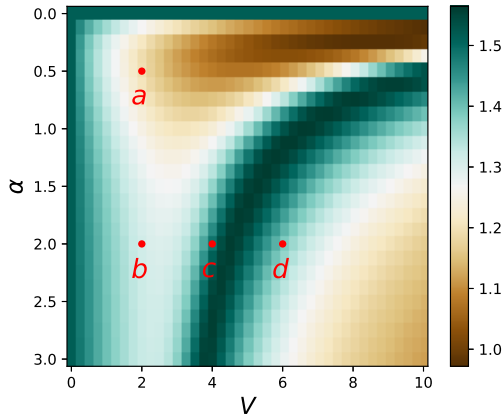


FIG. 8. Distribution of the half chain entanglement entropy  $\mathcal{E}_{N/2}$  on the parameter domain  $(V, \alpha) \in [0, 10] \times [0, 3.0]$  divided into  $40 \times 24$  grids for system size  $N = 100$ . Several dots are marked  $a, b, c$  and  $d$  whose scaling of entanglement are shown in Fig.9.

ranges.

### C. entanglement entropy

In the above, we have determined the approximate ground state phase diagram at half filling. It is also interesting to study quantum entanglement in the ground states, since it provides alternative characterization of many body wave function and may have interesting connection with quantum phase transitions<sup>29</sup>.

We use the von Neumann entanglement entropy as a measure of bipartite entanglement between the subsystems residing on the left  $L$  sites of the chain and that on the remaining right  $N - L$  sites, which is formulated by

$$\mathcal{E}_L = -\text{Tr}(\rho_L \log_2(\rho_L)), \quad (8)$$

and where  $\rho_L = \text{Tr}_{[L+1, N]}(|\psi\rangle\langle\psi|)$  is the reduced density matrix of the left subsystem, by tracing out the right one.

Fig.8 displays an overview of the distribution of half chain entanglement  $\mathcal{E}_{N/2}$  on the parameter space for  $N = 100$ . Two features can be noted: First, all points on the boundary lines of  $V = 0$  and  $\alpha = 0$  take same values of entanglement and the values are relatively high, since they are identically free fermions. Second, there is an extended peak of entanglement in the middle of the figure. Let us denote by  $V_p$  the location of the peak for a given  $\alpha$ . Then the curve  $V_p(\alpha)$  has the same trend as  $V_c(\alpha)$ . This supports previous conclusions about the phase diagram, and  $V_p$  should have intimate connections with  $V_c$ . Since  $V_p$  can be easily obtained, one may wonder can it be used to precisely locate the later. In short, the answer is no. For example, at  $\alpha = 3.0$  and  $N = 100$ ,  $V_p = 3.84$  is much larger than  $V_c \simeq 2.65$ . Although  $V_p$  relies on  $N$  and will scale closer to  $V_c$  as system size  $N$  increases, extrapolation of  $V_p$  using very large  $N$  can still hardly

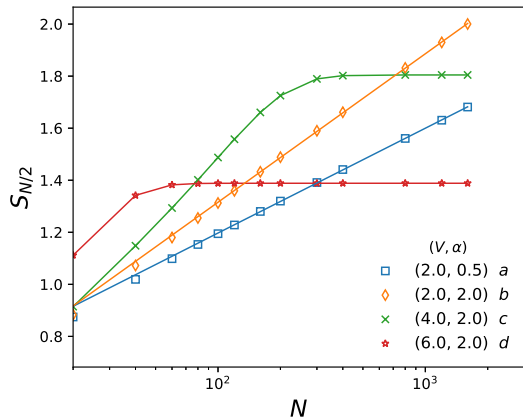


FIG. 9. Scaling of half chain entanglement  $\mathcal{E}_{N/2}$  versus systems size  $N$  for several  $(V, \alpha)$  pairs, with  $N$  as large as 1600. These pairs are labeled  $a, b, c$ , and  $d$ , whose positions are also shown in Fig.8. Lines for  $a$  and  $b$  are fitting to the relation  $\mathcal{E}_{N/2} \sim \frac{c}{6} \log_2(N)$ , yielding the coefficient  $c = 0.73$  and  $1.03$ , respectively. Lines for  $c$  and  $d$  are guide for eyes.

reach  $V_c$ . (This has been demonstrated for the  $XXZ$  model in Ref.30 and persists also for finite  $\alpha$  which we did not show at here). The reason for the existence of the peak is explained in the next paragraphs. We argue that  $V_p$  remains a good, strict upper bound on  $V_c$ .

Further understanding of entanglement structure of the system can be gained by analyzing scaling of  $\mathcal{E}_L$  with subsystem size  $L$ . For gapped and SR systems  $\mathcal{E}_L \sim \text{const.}$ , when  $L$  is greater than the correlation length. This is the well known area law of entanglement for 1D<sup>31,32</sup>. Whereas for gapless ones,  $\mathcal{E}_L$  should (slowly) diverge with increasing  $L$ . It is interesting to check whether this paradigm is altered or not when LR interactions present.

Instead of fixing a  $N$  and studying the relation of  $\mathcal{E}_L$  with  $L$ , we choose to fix the ratio  $L/N = 1/2$  and analyze the scaling of  $\mathcal{E}_{N/2}$  with  $N$ . The later has the benefit that only one parameter is needed. Fig.9 shows the results in a log-linear plot for 4 points in the  $V$ - $\alpha$  plane. They are marked  $a, b, c$  and  $d$  in Fig.8 and are representatives of different phases. Points  $c$  and  $d$  are both in the CDW phase, and entanglement saturates for large enough  $N$  as expected. Point  $b$  is in the Luttinger liquid phase, and entanglement diverges logarithmically. The interesting case is point  $a$  which is in the WC phase. It has a finite charge gap, but entanglement still diverges logarithmically. The two points  $b$  and  $a$  have different slope in the logarithmic scalings. One may extract an effective central charge for each of them by fitting with the formula  $\mathcal{E}_{N/2} \sim \frac{c}{6} \log_2(L)$ , which gives  $c = 1.03$  and  $0.73$  respectively. The former matches well with the theoretical value of 1, while the later shows again deviation from Luttinger liquid. When entering from the metallic phase (point  $b$ ) to the insulating phase (points  $c$  and  $d$ ), opening of a small gap leads to faster growth of entan-

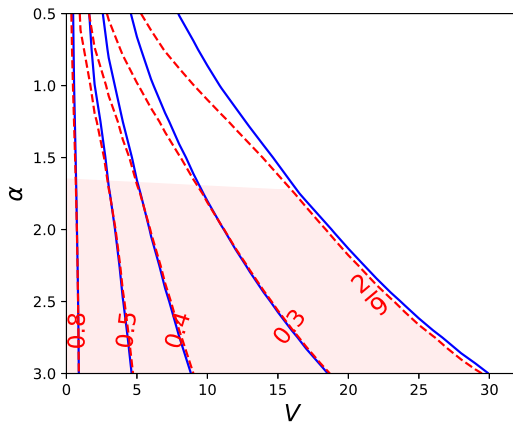


FIG. 10. Contour plot of correlation exponents  $K_1$  (solid) and  $K_2$  (dashed) restricted to  $K_1, K_2 \geq \frac{2}{9}$ . They are extracted in the same way as in Fig.2 and 3. In this section all results are for  $n = 1/3$ .

gument (comparing  $b$  and  $c$ ), while too large gap leads to too soon saturation of entanglement (comparing  $c$  and  $d$ ). It is these two competing effects that caused the peak of entanglement near  $c$  (for  $N = 100$ ) in Fig.8.

In short, the results of entanglement fully support the conclusions ahead. And LR interactions do not lead to very large entanglement and more complicated ground states in the model.

#### IV. $n=1/3$ PHASE DIAGRAM

In this section we study the ground states for filling  $n = 1/3$ . We measure some quantities in parallel with  $n = 1/2$  and compare their results. To begin with, the correlation exponents  $K_1$  and  $K_2$  are calculated in the same way as before and contour plots of them are shown in Fig.10. One can see that they agree well in the lower left region of the  $V$ - $\alpha$  plane, demarcating the Luttinger liquid region. The  $K$  values clearly decrease as  $\alpha$  goes down from 3.0 in this region. So, compared with  $n = 1/2$ , LR interactions have more salient effects on the renormalized  $K$  values. When  $\alpha$  is very small,  $K_1$  and  $K_2$  are obviously different, indicating breakdown of Luttinger liquid. It is difficult to determine a critical value  $\alpha_c$  for when this occurs. Then the boundary between Luttinger liquid and Wigner crystal is only roughly estimated to be  $1.0 \leq \alpha_c < 2.0$  and it may depend on  $V$ . The right boundary of Luttinger liquid phase is determined unambiguously by the critical value  $K_c = 2/9$ . For reference,  $V_c$  are 29.8 and 18.2 for  $\alpha = 3.0$  and 2.0, respectively.

Next we analyse the metal-insulator transition. For  $n = 1/2$ , the transition has been characterized by the occurrence of the CDW order through the scaling of the  $2k_F$  peak of the structure factor. This is, however, not quite applicable for  $n = 1/3$ . The reason is that there are oscillations (the Friedel oscillation) in local density of

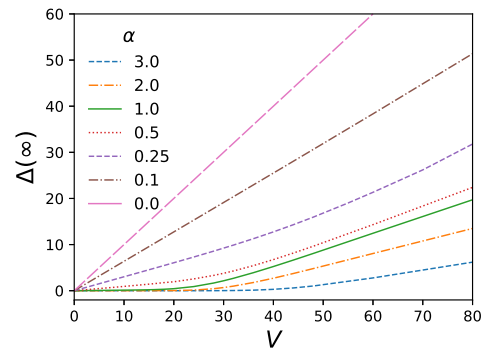


FIG. 11. Extrapolated single particle charge gap  $\Delta(\infty)$  as a function of  $V$  for different  $\alpha$ . The values of  $\Delta(\infty)$  are extracted in the same way as that for Fig.6.

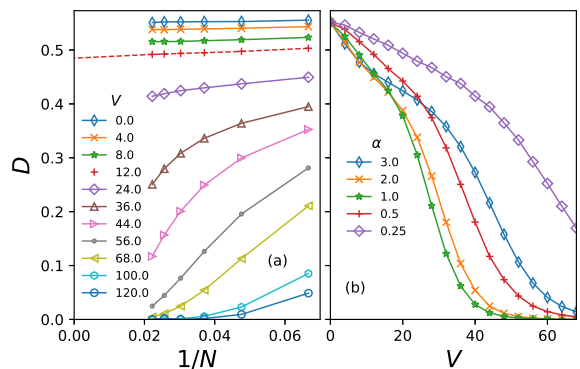


FIG. 12. (a) Charge stiffness  $D$  vs.  $1/N$  at  $\alpha = 0.5$  and for different interaction strength  $V$ . The system sizes are  $N = 15, 21, 27, 33, 39$  and  $45$ , corresponding to odd numbers of fermions. Solid lines at are guide to eye. Dashed line at  $V = 12.0$  is fit to a third order polynomial in  $1/N$ . (b)  $D$  as a function of  $V$  for different  $\alpha$ , obtained at a fixed finite system size of  $N = 45$ . These data are obtained through DMRG with periodic boundary conditions and the bond dimensions used are up to 640.

fermions  $\langle \hat{n}_i \rangle$  in a finite size system with OBC. Besides, the oscillation may decay in a power law in the metallic phases, which will not damp out for long distances, as a result it is difficult to distinguish it with a true CDW order by extrapolation in system sizes (we refer to 33 for detailed discussion of Friedel oscillation for lattice models).

Fig.11 shows the extrapolated single particle charge gap  $\Delta(\infty)$  as a function of  $V$  for different  $\alpha$ . Like  $n = 1/2$ , two different behaviours appear, which are separated by  $\alpha = 1$ . For each  $\alpha > 1$ ,  $\Delta(\infty)$  becomes nonzero at certain  $V_c$ , which reduces for smaller  $\alpha$ . This shows shrinking of the metallic region as interaction range increases. While in the range of  $0 \leq \alpha \leq 1$ , it is always gapped except at  $V = 0$ ; Besides  $\Delta(\infty)$  is proportional to  $V$  in the beginning and later increases with  $V$  with a larger slope for a given  $\alpha$  (this is obvious for  $\alpha = 1.0$  and

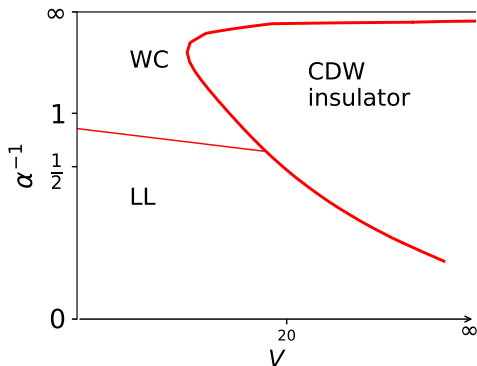


FIG. 13. Possible phase diagram as a function of  $V$  and inverse of  $\alpha$  for  $n = 1/3$ . The thick solid line indicates the boundary between metallic phases with the CDW insulator phase. The critical value  $V_c \rightarrow \infty$  as  $\alpha$  approaches 0 or  $\infty$ . The thin solid indicates a transition between the Luttinger liquid phase (LL) and Wigner crystal (WC) phase. In addition, entire lines of  $V = 0$  or  $\alpha = 0$  belong to the Luttinger liquid phase.

0.5, but is hidden for smaller  $\alpha$  due to restriction of the range of  $V$  in the figure), which may indicate change from WC to the CDW phase. One also notes that  $\Delta(\infty) = V$  at  $\alpha = 0$ , which is independent of band-filling.

The gapped region at  $0 \leq \alpha \leq 1$  and small  $V$  is actually metallic. This is supported by the study of the charge stiffness, as has been made for  $n = 1/2$ . Fig.7(a) shows  $D$  vs.  $1/N$  for fixed  $\alpha = 0.5$  and different  $V$ . When  $V$  is small or large, finite size effects are weak. An extrapolation is performed for  $V = 12.0$ , leading to a finite value, which means the state is metallic. Similar conclusions can be reached for other parameters of  $\alpha$  and  $V$  in this region. Fig.12(b) compares dependence of  $D$  on  $V$  for different  $\alpha$ , with a fixed finite system size of  $N = 45$ . For each  $\alpha$ ,  $D$  decreases from around the theoretical value  $\sqrt{3}/\pi$  at  $V = 0$  to zero at some large enough  $V$ , indicating a metal-insulator transition. Decrease of  $D$  to zero becomes faster when  $\alpha$  changes from 3.0 to 1.0, while becomes slower when  $\alpha$  continues changing from 1.0 to 0.25. This finite size result implies that the metallic region may first shrink and then expand as the interaction range increases.

Combining the above results of the Luttinger parameter, charge gap and charge stiffness, one can infer that dependence of the transition point  $V_c$  on  $\alpha$  is not monotonic.  $V_c$  should first decrease then, at some value of  $\alpha$ , turns to increase, as  $\alpha$  reduces. The location of the turning point should be no larger than 1. Note also that theoretically there is no transition at  $\alpha = \infty$  or  $\alpha = 0$  for for  $n = 1/3$ . Then a possible phase diagram is summarized in Fig.13. It is in essence consistent with the phase diagram for  $n = 1/2$ . The main difference is that, in the large  $\alpha$  regime, fermions are much harder to be localized and LR interactions play a more pronounced role for the lower band-filling.

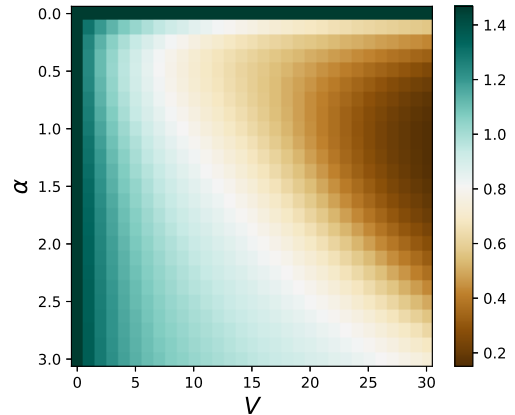


FIG. 14. Distribution of the half chain entanglement entropy  $\mathcal{E}_{N/2}$  on the parameter domain  $(V, \alpha) \in [0, 30] \times [0, 3.0]$  divided into  $30 \times 28$  grids for system size  $N = 96$ .

Fig.14 reveals the distribution of half chain entanglement on the  $V$ - $\alpha$  plane. A convex region in the middle right of the figure has lower entanglement, while the rest region on the left has higher entanglement. In contrast to  $n = 1/2$  there is no peak between the two regions. The left and right regions should correspond to metallic phases and the insulating phase, respectively, so the entanglement distribution correctly reflects the phase diagram shown above.

## V. COMPARISON WITH BOSONIZATION FORMULA

The metallic region with small  $\alpha$  is of special theoretical interests and practical relevance. Although bosonization technique has been extended for 1D fermions with Coulomb potential<sup>3,7,34</sup> and general power law interactions<sup>35-37</sup>, they are not as well established and widely checked as its application in short-ranged models. So we compare those analytical results with the numerical ones.

According to arguments from bosonization, for a generic interaction potential, it should be essentially short-ranged and falls in the Luttinger liquid phase if its Fourier transform is finite as  $q \rightarrow 0$ , otherwise it falls outside that phase<sup>3</sup>. In particular for the power law potential  $\mathcal{V}(r)$ , this means a critical value at  $\alpha_c = 1.0$ . Now, comparing with our results, the large  $\alpha$  region are indeed in the Luttinger liquid phase, while not for small  $\alpha$ . The difference is that the values of  $K_1$  and  $K_2$  seems diverge before  $\alpha$  reaches 1.0, signifying a larger  $\alpha_c$  than bosonization prediction. But this could also be a phenomenon at a crossover scale, and does not exclude the possibility that  $K_1$  and  $K_2$  may coincide for all  $\alpha > 1.0$  when measured at very large scales. We are not conclusive about the accurate location of  $\alpha_c$ .

Then we focus on the Coulomb potential  $\alpha = 1.0$ ,



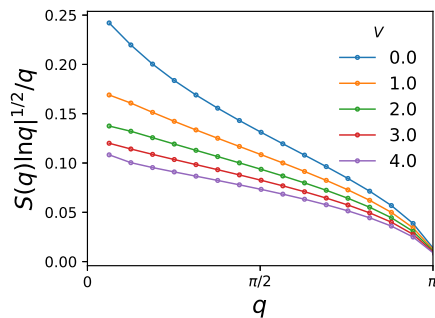


FIG. 15. Small momentum behaviour of the structure factor for  $\alpha = 1.0$  and several small values of  $V$  at  $n = 1/2$ .

which is certainly out of the Luttinger liquid phase. Main bosonization formula are summarized here for comparison. The Fourier transformed potential  $\mathcal{V}(q \rightarrow 0) \rightarrow \ln(1/q)$ , which leads to a plasmon dispersion,

$$\omega(q) \sim q \ln^{1/2}(1/q), \quad (9)$$

instead of a linear one as the Luttinger liquid. The density-density correlation and single particle Green's function are given respectively by the following two lines,

$$\langle \hat{n}_r \hat{n}_0 \rangle \sim \cos(2k_F r) \exp(-c_1 (\ln r)^{1/2}), \quad (10)$$

$$\langle \hat{c}_r^\dagger \hat{c}_0 \rangle \sim \exp(-c_2 (\ln r)^{3/2}). \quad (11)$$

The former decays slower than any power law and the later faster than any power law, which formally correspond to a Luttinger parameter  $K \rightarrow 0$ . Eq.(10) implies electrons are nearly ordered and can be interpreted as a metallic CDW state. In the above, we have shown that the  $K$  value reduces as  $\alpha$  gets smaller (see Figs.3 and 4). Both results agree qualitatively on the role of the LR interactions that they enhance (diagonal) density correlation while weaken the off-diagonal correlation, and that they deviate from standard Luttinger liquids.

To test the formulas in a quantitative level we follow the approaches of Refs.8, 9, and 12. They are compared with numerical results for only half filling and small interaction strengths. The dispersion relation can be tested via the Feynman formula, which means that the structure factor should behave as  $S(q) \sim q |\ln q|^{-1/2}$  at small momentum (in contrast to linear relation  $S(k) \sim qK$  for Luttinger liquid). Then the quantity  $S(q) |\ln q|^{1/2}/q$  would tend to a constant for small  $q$ . However, this is disapproved by our numerical results (see Fig.15). One may then test the density correlation by studying the scaling of the peak of structure factor with  $N$ , which should be well fitted by the relation  $S(2k_F) \sim N \exp(-c_1 \sqrt{\ln N})$ , if Eq.(10) were correct. However, again, we found the fitting are not satisfactory (not shown). Given that the density correlation is related to the dispersion relation, this is in fact no surprise and they should both hold or fail at the same time.

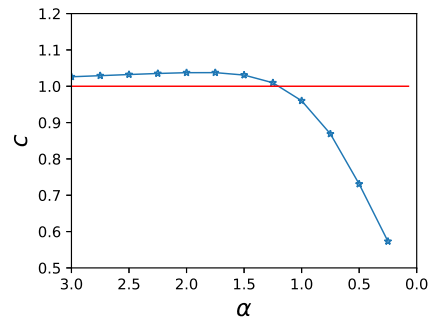


FIG. 16. Effective central charge  $c$  as a function of  $\alpha$  at  $V = 2.0$  and  $n = 1/2$ . The  $c$  values are extracted in the same way as in Fig.9 by fitting the scaling of entanglement with the relation  $\mathcal{E}_{N/2} \sim \frac{c}{6} \log_2(N)$ . The horizontal line of  $c = 1$  indicates the value of the central charge for the Luttinger liquid.

So we conclude that the bosonization results can only match with our DMRG data qualitatively but not quantitatively.

Finally, since some works have been interested in applying conformal field theory (CFT) to the model<sup>36,37</sup>, for reference we show the effective central charge  $c$  as a function of  $\alpha$  in Fig.16. It takes nearly constant values close to 1 for large  $\alpha$ , indicating preservation of the  $U(1)$ -invariant CFT of the Luttinger liquid, while varies continuously for smaller  $\alpha$ . This behaviour is well consistent with the previous analysis from Luttinger parameters.

## VI. CONCLUSION

In summary, we studied the ground states of 1D fermions with LR interaction decaying in a power law. We analyzed systematically the effects of interaction ranges on the ground state phases and transitions. In the large  $\alpha$  regime, the system is essentially short-ranged, where the paradigm of Luttinger liquid theory is still valid and the develop of metal-insulator transition point can be determined by the critical value of Luttinger parameter; In the small  $\alpha$  regime, the Luttinger liquid theory is breakdown, where the ‘‘Luttinger parameter’’ is scale dependent. Combining analysis on charge gap, order parameter and entanglement entropy, we obtained approximate phase diagram in the whole parameter plane and discussed the impact of band filling on it.

The phase diagrams are in fact not very complicated, in some aspects even simpler than certain finite-ranged models<sup>38,39</sup>. This relies in the convexity of the potential  $\mathcal{V}(r)$  we have used, otherwise, other phases, such as the bond-order phase, will occur. The main conclusions were reached by comparing the correlation exponents extracted accurately in multiple ways within the DMRG/iDMRG techniques, which can be also applicable for other models. These results are relevant to ongoing experiments in quasi-1D conductor materials and

quantum simulators with trapped ions.

The bosonization formula agree with our quasi-exact results qualitatively, but not quantitatively. This may either indicates the former can not fully capture the low energy behaviour of the current model and elaboration in the formulation is needed, or for some other reasons, which needs be clarified in future studies on related models.

## ACKNOWLEDGEMENT

The author thanks prof. An-Min Wang for help with computation resources. This work was supported by Na-

tional Natural Science Foundation of China under Grant No. 11375168 and by Research Starting Fund of Xi'an Technological University.

## REFERENCES

- 
- <sup>1</sup> F. D. M. Haldane, *J. Phys. C: Solid State Phys.* **14**, 2585 (1981).
  - <sup>2</sup> J. Voit, *Rep. Prog. Phys.* **58**, 977 (1995).
  - <sup>3</sup> T. Giamarchi, *Quantum physics in one dimension*, Vol. 121 (Oxford university press, 2004).
  - <sup>4</sup> A. R. Goni, A. Pinczuk, J. S. Weiner, J. M. Calleja, B. S. Dennis, L. N. Pfeiffer, and K. W. West, *Phys. Rev. Lett.* **67**, 3298 (1991).
  - <sup>5</sup> H. Steinberg, O. M. Auslaender, A. Yacoby, J. Qian, G. A. Fiete, Y. Tserkovnyak, B. I. Halperin, K. W. Baldwin, L. N. Pfeiffer, and K. W. West, *Phys. Rev. B* **73**, 113307 (2006).
  - <sup>6</sup> V. V. Deshpande and M. Bockrath, *Nature Physics* **4**, 314 (2008).
  - <sup>7</sup> H. J. Schulz, *Phys. Rev. Lett.* **71**, 1864 (1993).
  - <sup>8</sup> M. Casula, S. Sorella, and G. Senatore, *Phys. Rev. B* **74**, 245427 (2006).
  - <sup>9</sup> L. Shulenburger, M. Casula, G. Senatore, and R. M. Martin, *Phys. Rev. B* **78**, 165303 (2008).
  - <sup>10</sup> G. E. Astrakharchik and M. D. Girardeau, *Physical Review B* **83**, 153303 (2011), arXiv: 1101.0103.
  - <sup>11</sup> G. Ferré, G. E. Astrakharchik, and J. Boronat, *Phys. Rev. B* **92**, 245305 (2015).
  - <sup>12</sup> G. Fano, F. Ortolani, A. Parola, and L. Ziosi, *Phys. Rev. B* **60**, 15654 (1999).
  - <sup>13</sup> M. Hohenadler, S. Wessel, M. Daghofer, and F. F. Assaad, *Phys. Rev. B* **85**, 195115 (2012).
  - <sup>14</sup> D. Poilblanc, S. Yunoki, S. Maekawa, and E. Dagotto, *Phys. Rev. B* **56**, R1645 (1997).
  - <sup>15</sup> S. Capponi, D. Poilblanc, and T. Giamarchi, *Phys. Rev. B* **61**, 13410 (2000).
  - <sup>16</sup> W. C. Campbell, C. Monroe, E. E. Edwards, R. Islam, D. Kafri, S. Korenblit, A. Lee, P. Richerme, C. Senko, and J. Smith, *Ion Traps for Tomorrows Applications* **189**, 169 (2015).
  - <sup>17</sup> S. R. White, *Phys. Rev. Lett.* **69**, 2863 (1992); *Phys. Rev. B* **48**, 10345 (1993).
  - <sup>18</sup> G. M. Crosswhite, A. C. Doherty, and G. Vidal, *Phys. Rev. B* **78**, 035116 (2008).
  - <sup>19</sup> F. Fröwis, V. Nebendahl, and W. Dür, *Phys. Rev. A* **81**, 062337 (2010).
  - <sup>20</sup> J. Dukelsky, M. A. Martín-Delgado, T. Nishino, and G. Sierra, *Europhys. Lett.* **43**, 457 (1998); F. Verstraete, D. Porras, and J. I. Cirac, *Phys. Rev. Lett.* **93**, 227205 (2004); I. P. McCulloch, *J. Stat. Mech. Theor. Exp.* **2007**, P10014 (2007); U. Schollwöck, *Ann. Phys.* **326**, 96 (2011).
  - <sup>21</sup> I. P. McCulloch, arXiv:0804.2509 [cond-mat] (2008).
  - <sup>22</sup> S. Daul and R. M. Noack, *Phys. Rev. B* **58**, 2635 (1998); R. T. Clay, A. W. Sandvik, and D. K. Campbell, *Phys. Rev. B* **59**, 4665 (1999); S. Ejima, F. Gebhard, and S. Nishimoto, *Europhysics Letters (EPL)* **70**, 492 (2005).
  - <sup>23</sup> C. Karrasch and J. E. Moore, *Phys. Rev. B* **86**, 155156 (2012).
  - <sup>24</sup> T. D. Kühner, S. R. White, and H. Monien, *Phys. Rev. B* **61**, 12474 (2000).
  - <sup>25</sup> E. H. Lieb and F. Y. Wu, *Physical Review Letters* **20**, 1445 (1968).
  - <sup>26</sup> W. Kohn, *Phys. Rev.* **133**, A171 (1964).
  - <sup>27</sup> R. Resta, *J. Phys.: Condens. Matter* **14**, R625 (2002).
  - <sup>28</sup> Here multiple factors have severely restricted evaluation of  $D$  accurately for only small  $N$ : (i) use of periodic boundary conditions, (ii) then inapplicability of the MPO technique for approximating LR interactions, (iii) evaluation of the second order derivative in Eq.7 being very numerical delicate.
  - <sup>29</sup> L. Amico, R. Fazio, A. Osterloh, and V. Vedral, *Rev. Mod. Phys.* **80**, 517 (2008).
  - <sup>30</sup> B. Wang, M. Feng, and Z.-Q. Chen, *Phys. Rev. A* **81**, 064301 (2010).
  - <sup>31</sup> J. Eisert, M. Cramer, and M. B. Plenio, *Rev. Mod. Phys.* **82**, 277 (2010).
  - <sup>32</sup> M. B. Hastings, *J. Stat. Mech. Theor. Exp.* **2007**, P08024 (2007).
  - <sup>33</sup> S. R. White, I. Affleck, and D. J. Scalapino, *Phys. Rev. B* **65**, 165122 (2002).
  - <sup>34</sup> D. W. Wang, A. J. Millis, and S. Das Sarma, *Phys. Rev. B* **64**, 193307 (2001).
  - <sup>35</sup> A. Iucci and C. Naón, *Phys. Rev. B* **61**, 15530 (2000).
  - <sup>36</sup> C. M. Naón, M. J. Salvay, and M. L. Trobo, *Phys. Rev. B* **72**, 245110 (2005).
  - <sup>37</sup> H. Inoue and K. Nomura, *J. Phys. A: Math. Gen.* **39**, 2161 (2006).
  - <sup>38</sup> T. Mishra, J. Carrasquilla, and M. Rigol, *Phys. Rev. B* **84**, 115135 (2011).
  - <sup>39</sup> S. Ejima, F. Gebhard, S. Nishimoto, and Y. Ohta, *Phys. Rev. B* **72**, 033101 (2005).